THE JOURNAL OF PHYSICAL CHEMISTRY B

Article

pubs.acs.org/JPCB

Structure and Stability of Phospholipid Bilayers Hydrated by a Room-Temperature Ionic Liquid/Water Solution: A Neutron Reflectometry Study

Antonio Benedetto,[*,†] Frank Heinrich,[‡,§] Miguel A. Gonzalez,[∥] Giovanna Fragneto,[∥] Erik Watkins,[∥,⊥] and Pietro Ballone[⊗,#]

[†]School of Physics, University College Dublin—UCD, Belfield Campus, Dublin 4, Ireland

[‡]Department of Physics, Carnegie Mellon University, Pittsburgh, Pennsylvania 15213, United States

[§]Center for Neutron Research, National Institute of Standards and Technology, Gaithersburg, Maryland 20899, United States

[∥]Institute Laue-Langevin, Grenoble, France

[⊥]Lujan Neutron Scattering Center, Los Alamos National Laboratory, Los Alamos, New Mexico 87545, United States

[⊗]Center for Life Nano Science @Sapienza, Istituto Italiano di Tecnologia (IIT), 00161 Roma, Italy

[#]Department of Physics, Universita' di Roma "La Sapienza", 00185 Roma, Italy

Supporting Information

ABSTRACT: Neutron reflectometry (NR) measurements were carried out to probe the structure and stability of two model biomembranes consisting of 1-palmitoyl-2-oleoyl-*sn*-glycero-3-phosphocholine (POPC) and 1,2-dimyristoyl-*sn*-glycero-3-phosphatidylcholine (DMPC) phospholipid bilayers hydrated by water solutions of two prototypical room-temperature ionic liquids (RTILs), namely, 1-butyl-3-methyl-imidazolium chloride ([bmim][Cl]) and choline chloride ([Chol][Cl]) at concentrations of 0.1 M and 0.5 M, respectively. The raw data were analyzed by fitting a distribution of scattering length densities arising from the different chemical species in the system. The results of this analysis show that (a) for all systems and concentrations that we considered, the thickness of the bilayers shrinks by ∼1 Å upon dissolving the ionic liquid into water and that (b) the RTIL ions enter the bilayer, finding their way to a preferred location in the lipid range that is nearly independent of the lipid and of the $[bimim]^+$ or $[Chol]^+$ choice. The volume fraction of RTIL sorbed in/on the bilayer, however, does depend on the lipid, but, again, is the same for [bmim][Cl] and for [Chol][Cl]. Thus, the RTIL occupies ∼5% of the bilayer volume in POPC, rising to ∼10% in DMPC. Repeating the measurements and data analysis after rinsing in pure water shows that the changes in the bilayer due to the RTIL sorption are irreversible and that a measurable amount of IL remains in the lipid fraction, that is, ∼2.5% of the bilayer volume in POPC and ∼8% in DMPC.

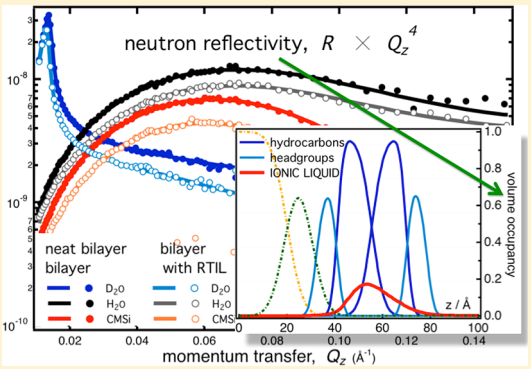

INTRODUCTION

Room-temperature ionic liquids (RTILs) represent a vast class of ionic compounds, usually consisting of an organic cation and an organic or inorganic anion, whose melting temperature falls below the conventional limit of 100 °C.[1]

The interest in these systems has been fuelled by a wide range of applications[2,3] that have been proposed over the years, including the replacement of more volatile solvents in industrial chemical processes,[4,5] the fabrication of lubricants[6,7] suitable for high temperature/high pressure conditions, the design of innovative electrochemical devices[8−11] having RTILs has their fluid electrolyte component, and even the sequestration of CO_2 from power-generation stacks.[12] Arguably, the properties that most contributed to raise expectations in RTILs are their perceived safety and their low impact on the environment.[13−15]

Indeed, several years of extensive use in research centers and in small-scale industrial processes confirm the general assessment of low toxicity and relatively easy and safe handling of these compounds. However, the prospect of greatly expanding the scale and scope of RTIL applications, and especially the exploration of their use as active pharmaceutical ingredients[16] or as excipients in drugs formulation, impose a deeper and stricter analysis of potential health effects of RTILs.[17]

Surprisingly, this crucial aspect of RTIL compounds has until now received only limited attention, and the discussion has been split between the alarming observation of toxicity toward cell cultures,[18] microorganisms[19] or higher organisms,[20,21] and the

Received: July 29, 2014
Revised: September 18, 2014
Published: September 24, 2014

reductive view that there is no reason for concern. A refreshing variation on these arguments has been the observation that RTILs could play an unexpected positive role as potent antibiotics.[22−27]

Recently, the characterization of RTIL toxicology and, in general, of health effects by biological essays, has been significantly broadened to include the experimental investigation of RTILs interacting with prototypical biological structures such as proteins, nucleic acids, and phospholipid bilayers, carried out using chemical physics approaches.

For instance, early studies performed by spectroscopy[28] and by electrochemical means[29,30] probed the enzymatic activity of cytochrome c in RTILs, suggesting a complementary but still important role of RTILs in biocatalysis.

Luminescence measurements, nuclear magnetic resonance (NMR), light scattering, and transmission electron microscopy imaging highlighted the opposite effects of tetramethylammonium mesylate [TMA][Mesyl] and of tetramethylguanidinium acetate [TMG][AcO] on the self-assembly of lysozyme into amyloid fibrils. While [TMA][Mesyl] enhances lysozyme fibrillation,[31] [TMG][AcO] prevents the formation of fibrils.[32] Tetramethylammonium nitrate (EAN), moreover, is able to dissolve mature amyloid fibers[31] into individual proteins that upon solvation even recover their enzymatic activity. These results provide a factual basis for future applications of RTILs not only in pharmacology but also in nanotechnology.[33]

UV spectroscopy and again NMR measurements have demonstrated the effect of RTILs based on the alkylammonium cation to affect the relative stability of G-C and T-A base pairs in DNA,[34] while chromophore binding and luminescence measurements have highlighted the long-term stability of DNA in hydrated ionic liquids,[35] potentially providing a simple and inexpensive technique to preserve biological samples at room temperature.

In the context of biological effects, the interaction of RTILs with lipid-based structures arguably is the most relevant case, since the first encounter of a foreign chemical species with a living cell is likely to occur at its protective biomembrane, which primarily consists of a phospholipid bilayer.

This intuitive consideration is supported by the observation that the cytotoxicity of RTILs measured by a variety of bioassay approaches shows a clear positive correlation with their lipophilicity.[17,23,36]

Atomic force microscopy (AFM),[37] luminescence,[38] and quartz microbalance[39] approaches have been used to investigate the stability and structure of phospholipid vesicles and of solid-supported bilayers in a water solution of RTILs made primarily but not exclusively of the imidazolium cation and a sequence of anions of increasing hydrophobicity. The results reveal important specific interactions of phospholipids and organic ionic species, once again pointing to potential toxicity toward cells, but also suggesting a possible role of RTILs in medical applications.

Imidazolium cations $[C_n\text{mim}]^+$ with n = 4, 6, or 8 carbon atoms in their alkyl tails, for instance, have been shown to promote the permeability of bilayers made of saturated and (slightly) unsaturated phospholipids. The smallest cation ($[\text{bmim}]^+$, $n = 4$) only causes limited leakage from localized holes in the bilayers, while larger cations with n = 6 and 8 carbon atoms in their alkyl tail give rise to permeability already at low RTIL concentration, and fully disrupt the bilayer at high (200 mM) concentration. The drastic increase of the RTIL effect with increasing alkyl tail length suggests that solvation of the cation tail into the neutral portion of the phospholipid bilayer is the major factor in the RTIL/lipid mutual affinity.

Stimulated by these works, computer simulation studies have been carried out to investigate the microscopic mechanisms underlying the experimental observations.[40,41] Analysis of trajectories from molecular dynamics simulations of phospholipid bilayers floating in water solutions of [bmim][Cl], [bmim][PF_6], and [bmim][Tf_2N] shows that the first incorporation of RTIL cations ($[\text{bmim}]^+$) into the bilayer occurs on the time scale of 100 ps, and the system reaches a condition of local equilibration within 10−20 ns, which lasts over the ∼150 ns covered by simulation. No simulation result is available on significantly longer time scales or for system sizes exceeding a few hundred lipids and 2000 Å^2 cross area, which are relevant for the extraction and solvation of lipid molecules by RTILs, for the formation of pores, and for the global destabilization of the lipid bilayer at high RTIL concentration. Perhaps more importantly, $[\text{bmim}]^+$ is the only cation that has been considered in these computational studies. Recent additions[42,43] to the short list of computational investigations of these systems have somewhat extended and confirmed the picture provided by the early[40,41] simulation studies.

Whenever a comparison is possible, the simulation results turn out to be fully consistent with the experimental picture and reveal the peculiar role of the anion solubility. Small, hydrophilic anions such as $[Cl]^-$ remain in water solution and limit the amount of cations that can be incorporated into the bilayer. Introducing anions of lower water affinity such as $[PF_6]^-$ causes the deposition of a molecularly thin film of anions at the water/lipid interface, in close contact with the ionic portion of cations, and with the polar groups in the lipid head. RTILs based on large, hydrophobic anions such as $[Tf_2N]^-$ cause the precipitation of the ionic component into mesoscopic droplets that tend to adsorb at the bilayer/water interface.

Although interesting, these studies are in many ways limited in the information that they can provide. For instance, luminescence and quartz microbalance measurements do not offer explicit structural information. On the other hand, AFM and simulation provide a view of the RTIL and phospholipid conformation that is too local to answer the first basic questions that arises in this context, concerning the global stability, structure, and dynamics of a phospholipid bilayer in a water environment in which RTILs have been dissolved at moderate concentration. Last but not least, a few of the experimental methods applied until now such as AFM or transmission electron microscopy perturb the system through forces whose strength cannot be reduced at will.

To overcome these limitations, we resort to neutron scattering reflectometry (NR), whose ability to determine the system structure perpendicular to a reference surface while probing a wide area represents crucial aspects for our investigation.[44,45] The weak interaction of neutrons with the atomic nuclei ensures that NR provides a faithful picture of the system under study, unperturbed by the measurement. The concentration profile of the different chemical components present in the system can be determined by applying isotopic substitution, which represents an option unavailable to other experimental techniques such as X-ray reflectometry. On the other hand, the successful application of both X-ray and neutron reflectometry requires homogeneous and well-oriented bilayers deposited on solid surfaces of low roughness.

In the present study, we apply NR in its specular reflectivity flavor to analyze 1-palmitoyl-2-oleoyl-*sn*-glycero-3-phosphocholine (POPC) and 1,2-dimyristoyl-*sn*-glycero-3-phosphatidylcholine

(DMPC)[46] phospholipid bilayers supported on a silica substrate. The fluid side of the interface is represented by water solutions of [bmim][Cl] and [Chol][Cl], selected because of their prototypical role, good solubility, and availability of experimental data on their basic chemical physics properties. Both cations, that is, $[bmim]^+$ and $[Chol]^+$, are fairly bulky ions, whose size reduces the strength of their Coulomb interaction and enhances their dispersion forces, thus pointing to an easy incorporation into the phospholipid bilayer, whose amphiphilic character provides suitable conditions to solvate both ionic and neutral species. Choline, moreover, is a common player in metabolic pathways, and is part of the polar head of phospholipids belonging to the phosphatidylcholine and sphingomyelin families, thus enhancing the relevance of our results for biochemical applications. The phospholipid deposition on the solid substrate breaks the symmetry of the two leaflets in the bilayer, and in a few instances we will make a distinction between the results for the inner leaflet, closest to the silica surface, and the outer leaflet, farthest from silica.

Our data show that for all the systems that we have studied: (a) the RTIL water solutions do not disrupt the global integrity of the bilayers, whereas (b) the thickness of the bilayers shrinks by ∼1 Å upon dissolving the IL into water at either 0.1 or 0.5 M concentration. (c) An important amount of RTIL is sorbed in/on the bilayer; the volume fraction of the absorbed RTILs does depend on the lipid, but it is independent of the cation choice: both for $[bmim]^+$ and for $[Chol]^+$, the RTIL occupies ∼5% of the bilayer volume in POPC, rising to ∼10% in DMPC. (d) The quantitative determination of the concentration profile of the RTILs into the membrane is challenging, but our results show that it is similar in all the four systems that we considered. (e) The repetition of the measurements and data analysis after rinsing the sample in pure water shows that, to some extent, the changes in the bilayer due to the RTIL absorption are irreversible and that an important amount of IL remains in the bilayers, that is, ∼2.5% of the bilayer volume in POPC and ∼8% in DMPC.

The neutron reflectivity measurements whose results are presented and discussed in the following sections were carried out both at the National Institute of Standards and Technology (NIST), Gaithersburg, USA, and at the Institute Laue-Langevin (ILL), Grenoble, France.

The positive outcome of the present study opens the way to a systematic analysis of the sorption of organic ionic species onto phospholipid bilayers, providing a first quantitative screening of potential biological effects of RTIL.

The results, moreover, support the validity and reliability of the simulation results for closely related systems[40−43] and show that the combination of neutron reflectometry and molecular dynamics simulation provides a sensitive and accurate tool to investigate the effect of RTILs on phospholipid membranes.

EXPERIMENTAL SECTION

The aim of our study is the experimental investigation of the interaction of RTIL species in water solution with phospholipid bilayers, probed at the molecular scale. More specifically, the effect of two RTILs, namely, [bmim][Cl] and [Chol][Cl], on two model biomembranes, namely, POPC and DMPC, was investigated by means of specular neutron reflectometry (NR). Measurements were carried out at two different instruments: the reflectometer MAGIK at NIST,[47] and the high-flux horizontal reflectometer Fluid Interfaces Grazing Angles ReflectOmeter (FIGARO) at ILL.[48]

In the MAGIK case, reflectivity curves were recorded for momentum transfer values between 0 and 0.25 $Å^{-1}$ with an instrumental wavelength resolution ($d\lambda/\lambda$) = 1%. A flow cell was used that holds 3″ diameter Si wafers and allows for in situ sample manipulation on the instrument. Therefore, subsequent measurements were performed on exactly the same sample area. The entire flow cell was maintained at room temperature.

In the FIGARO case, the intensity of specular reflected neutrons of incoming wavelengths between 2 and 20 Å at the two incident angles of 0.8° and 3.2° was measured, giving access to a momentum transfer normal to the surface in the range from 0.0045 to 0.25 $Å^{-1}$ (i.e., down-reflection mode). The instrumental wavelength resolution ($d\lambda/\lambda$) is 7%. The sample cells consist of 10 × 5 × 1 cm^3 silicon blocks in contact with a water reservoir, clamped between thermalized aluminum holders.

On both instruments, the lipid bilayer is absorbed onto the 10 × 5 cm^2 surface of the silicon substrate, and the cell is filled with the solvent (about 2 mL), consisting of: (i) pure water in a first round of measurements, carried out to characterize the bilayer baseline behavior, (ii) water solutions of RTILs in the major production stage, and, finally, (iii) replaced again by pure water to check the reversibility of the RTIL sorption on or into the phospholipid bilayer.

Chemicals and Experimental Protocol. We purchased the fully hydrogenated h-DMPC (catalog no. 850345P), the d-DMPC with perduterated hydrocarbon chains and tails, that is, DMPC-d_{67}, (catalog no. 860348P), and the fully hydrogenated POPC (catalog no. 850457C) from Avanti Polar Lipids, Inc. (Birmingham, AL), and we purchased the [bmim][Cl] (catalog no. 04129- F) and the [Choline][Cl] (catalog no. C7017) from Sigma-Aldrich. Figure 1 reports the schematic structure of natural and deuterated DMPC, of POPC, and of the two RTILs.

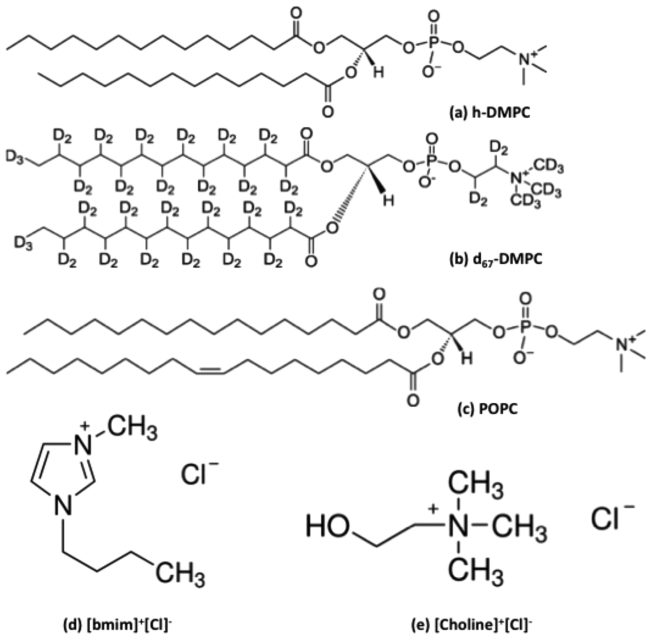

Figure 1. Schematic two-dimensional chemical structure of the lipids and of the ionic liquids considered in our study: (a) h-DMPC, (b) d_{67}-DMPC, (c) POPC, (d) [bmim][Cl], and (e) [Chol][Cl].

For the MAGIK experiments, Si wafers were cleaned with Micro-90 detergent, rinsed with Millipore water, immersed for 15 min in sulfuric acid with No-Chromix additive, rinsed with Millipore water, rinsed with ethanol, and dried in a stream of

dx.doi.org/10.1021/jp507631h | J. Phys. Chem. B 2014, 118, 12192−12206

nitrogen. Vesicles were prepared from 10 mg/mL POPC in chloroform. The chloroform solution was dried overnight under vacuum at 30 °C. The dry lipid film was resuspended in 10 mM NaH_2PO_4, 500 mM NaCl, pH 7.4 at a concentration of 5 mg/mL. The solution was sonicated for 70 min and remained milky. The milky solution was injected into the MAGIK wet cell containing the clean Si wafer (1.5 mL cell volume). After 60 min of incubation, the vesicle solution was replaced with 2 × 10 mL of 10 mM NaH_2PO_4, 50 mM NaCl, pH 7.4. The cell was flushed with 10 mL of heavy water for NR measurements on the neat bilayer. Water solutions of [bmim][Cl] at 0.1 M and 0.5M, and of [Chol][Cl] at 0.5 M, were prepared both in H_2O and D_2O. The complete list of the samples measured on MAGIK is reported in Table 1 of the Supporting Information.

For the FIGARO experiments, we prepared a solution of unilamellar vesicles by extrusion with 20 mg of lipid in 5 mL of pure water using the Avanti Mini-Extruder. During the extrusion process the solution was handled at 31 °C by using the heating block; this is crucial, since for vesicle preparation we need to work above the main-transition temperature (TM) of the bilayer, which in the case of DMPC is at 24 °C, that is, above room temperature. The resulting vesicle solution was diluted to a final concentration of 2 mg of DMPC per milliliter of water, and the temperature was adjusted to 31 °C before filling the sample cell, also held at 31 °C. In several minutes, the vesicles collapse at the silicon oxide surface and form a stable bilayer, separated from the solid surface by a thin water film. Water solutions of [bmim][Cl] at 0.5 M were prepared both in H_2O and D_2O. The complete list of the samples measured on FIGARO is reported in Table 1 of the Supporting Information.

All the experiments were performed above the main phase-transition temperature, that is, at ambient temperature for POPC on MAGIK, and at T = 31 °C for DMPC on FIGARO. NR data were collected by varying the contrast of both the solvent (i.e., by using H_2O/D_2O mixtures), and the lipid (i.e., by using both h-DMPC and d-DMPC). Data are also collected at three different stages of the sample manipulation: (i) before, (ii) during, and (iii) after the RTIL−bilayer interaction.

In a first stage, we characterized the properties of the neat bilayers, in contact with pure water (about 2 mL of water is needed to fill the experimental cell); in what follows, this condition is labeled as "neat bilayer before the interaction". Then, the pure water solvent hydrating the bilayers was replaced by water solutions of RTILs; these condition are labeled as "during the interaction". Finally, the pure water condition was restored by rinsing the system with about 10 mL of pure water. In all these stages, reflectivity spectra were collected according to the same experimental protocol.

Data Analysis Protocol. The raw data provided by our measurements represent the specular component $R(Q_z)$ of the neutron beam intensity reflected from the planar interface consisting of a lipid bilayer deposited on a silica surface and covered by water or by an RTIL water solution. The interface is oriented perpendicularly to the z axis, $R(Q_z)$ is normalized to the intensity of the incoming beam, the Q_z argument of $R(Q_z)$ represents the change of the neutrons wave vector upon reflection, given by

$$Q_z = \frac{4\pi}{\lambda}\sin\theta \tag{1}$$

where θ is the angle of incidence, and λ is the wavelength of neutrons in the beam.

Our aim is the determination of the composition or volume profile of the different chemical species across the interface, determined at sub-nanometer resolution. To achieve this goal, we follow standard approaches to relate $R(Q_z)$ to the z dependence of the scattering length density $\rho(z)$ (SLD), defined as

$$\rho(z) = \sum_{i\in\text{atoms}} b_i\delta(z - z_i) \tag{2}$$

where b_i is the scattering length of atom i.

In the kinematic (first Born) approximation, for instance:[49]

$$R(Q_z) = \frac{16\pi^2}{Q_z^{\,2}}|\rho(Q_z)|^2 \tag{3}$$

where $\rho(Q_z)$ is the Fourier transform of $\rho(z)$.

Inverting this relation to express $\rho(Q_z)$, or, equivalently, $\rho(z)$ in terms of $R(Q_z)$, however, is problematic, mainly because the information on the phase of $\rho(Q_z)$ is lost throughout the computation of the square modulus in eq 3. The problem could be solved under restrictive symmetry conditions, or, under weaker conditions, by a more complex method.[50]

A different route, however, relying on careful modeling and introducing volume and chemical constraints, offers a more intuitive approach, and for this reason it is widely used. The method can be described as follows. Since neutron reflectivity obeys the same rules of light reflectivity, the relation between $\rho(z)$ and $R(Q_z)$ can be established through the optical matrix method[51] and can be readily evaluated for any trial density $\rho(z)$ to give a trial $R(Q_z)$. Then, the mean square deviation of the trial and measured $R(Q_z)$ is minimized by standard (library) routines, progressively refining the trial $\rho(z)$. To carry out this task, we adopt the so-called composition-space approach,[52] modeling distributions of the following individual molecular groups: silicon oxide, substrate-proximal phosphocholine (PC) head groups, substrate-proximal methylene groups, substrate-proximal methyl groups, substrate-distal methyl groups, substrate-distant methylene groups, substrate-distal headgroups, and the RTIL cation. This analysis is far more detailed that in previous studies of lipids deposited on a solid substrate, in which the SLD of the interface is expressed in terms of slabs of constant scattering length density for the substrate, lipid, and solvent contributions only, without distinguishing the SLD of distinct chemical groups in the lipid subsystem. We verified that such a coarse representation of the total SLD does not allow us to determine the RTIL distribution at any acceptable degree of accuracy. Splitting the phospholipid contribution into its separate components lowers the χ^2 and allows us to identify the SLD due to the RTIL sorption at the lipid bilayer. The conditioning of the fit is strengthened by including constraints on the volume occupied by all the components, which cannot exceed the available space, as well as chemical constraints, preventing the spatial separation of components such as heads and tails that in fact are linked by covalent bonds. Volume and chemical constraints are ineffective for the anions, because of the relatively small size of Cl^-. For this reason, information on the anion distribution is conspicuously absent from our tables and figures.

In the composition-space approach, the density distribution of each component but the RTIL is represented by a boxcar function. Upon convolution with a Gaussian function accounting for thermal and conformational broadening, the z-dependence of the area covered by molecules or molecular fragments is given by the sum of two error functions. The RTIL cation distribution, less predictable than the others, is represented by a free-form monotonic Hermite spline,[53,54] defined by nine control points,

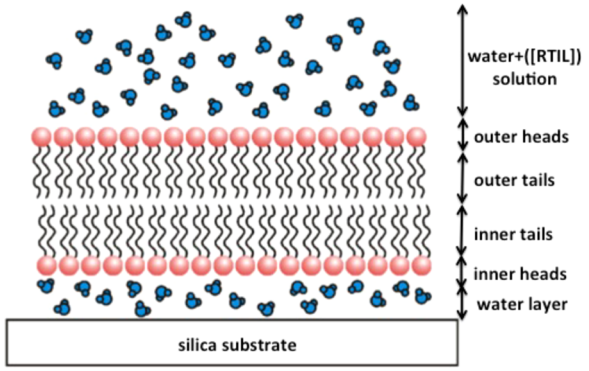

Figure 2. Schematic structure of solid-supported phospholipid bilayers.

and accounting for 16 additional free parameters in the scattering length profile modeling.

To disentangle the distribution of the different chemical components, we resort to isotopic substitution, as detailed in the previous subsection. The free parameters distributed in the functional form of the SLD $\rho(z)$ were determined by nonlinear χ^2 optimization carried out using the "GA_refl" and "Refl_1D" computer packages[55] developed at NIST. Error bars on the fit parameters were determined by repeating the fit on a population of computer-generated raw data, produced by a Monte Carlo Markov chain procedure[56] equivalent to the measured $R(Q_z)$ to within the 68% confidence level.

To accurately determine small variations in the fit parameters and in the system geometry resulting from the RTIL additions, all data sets concerning a given choice of the phospholipid bilayers are analyzed together, enhancing the accuracy of comparisons by cancellation of systematic errors.

On the other hand, the addition of several (16, see above) degrees of freedom in the fit to describe the RTIL distribution in space could partly compensate for the still-limited flexibility in the representation of the lipid and solvent distributions, producing in this way spurious results. To quantify this effect, we included a fictitious RTIL distribution also in the fit for the neat (i.e., without RTIL) samples. In the case of POPC and d-DMPC, the fit correctly attributed only a modest amplitude to the RTIL distribution. In the h-DMPC case, instead, the amplitude of the fictitious component turned out to be sizable, undermining the reliability of the data analysis. For this reason, in what follows and especially in the Supporting Information we report also the h-DMPC data, with, however, a major caveat that in this case the statistical error bars do not reliably measure the uncertainty of the results for the RTIL distribution.

Attributing a volume to each chemical group and molecular species[57−59] allows us to monitor the completeness of the space filling by the density distributions determined by the fit. Deviation from 1, that is, from completeness, could be attributed to the penetration of solvent into the lipid distribution and, thus, to a defective structure of the bilayer.

RESULTS AND DISCUSSION

As already stated, our study is aimed toward the investigation of how the presence of a small amount of RTILs in water solutions affects the structure and stability of phospholipid bilayers that, as it is well-known, are equilibrated by a competition of hydrophilic and hydrophobic interaction with water. A schematic view of the systems under investigation is shown in Figure 2, while Table 1 lists basic chemical physics properties of our systems. The most relevant information is the widespread scattering of length densities, which underlies the stability and accuracy of the data analysis.

In a first stage of our study, we carried out NR measurements on the neat bilayers, that is, DMPC and POPC, in water before the introduction of RTILs, both to validate our setup and method by comparison with benchmark data from the literature and to verify the quality of the bilayers resulting from our sample preparation. The neutron reflectivity of neat POPC and d-DMPC measured on MAGIK and FIGARO, respectively, in solvents of different H/D composition is shown in Figure 3a,b. The good separation of the curves obtained with different solvent contrast is apparent, opening the way to the accurate determination of structural parameters.

Table 1. Theoretical Scattering Length Densities (SLD) Calculated from the Neutron Scattering Length, *b*, of Each Atom, and Other Quantities of Interest

material	formula	MW (g/mol)	volume (A^3)	density (g/cm^3)	b (10^{-4} A)	SLD (10^{-6} A^{-2})
			Phospholipid Bilayers			
DMPC	$C_{36}H_{72}NO_8P$	677.945	1101	1.0225	3.11	0.282
DMPC-tail	$C_{26}H_{54}$	366.718	754	0.8076	−2.91	−0.386
DMPC-head	$C_{10}H_{18}NO_8P$	311.227	347	1.4894	6.01	1.732
d-DMPC	$C_{36}H_5NO_8PD_{67}$	745.345	1101	1.124	72.84	6.616
d-DMPC-tail	$C_{26}D_{54}$	421.042	754	0.9273	53.3	7.069
d-DMPC-head	$C_{10}H_5NO_8PD_{13}$	324.305	347	1.552	19.54	5.631
POPC	$C_{42}H_{82}NO_8P$	760.076	1246	1.013	3.34	0.268
POPC-tail	$C_{32}H_{64}$	448.799	925	0.804	−2.66	−0.287
POPC-head	$C_{10}H_{18}NO_8P$	311.277	321	1.610	6.01	1.87
			Water Contrasts			
H_2O	H_2O	18	30	0.997	−0.167	−0.56
CMSi	H_2O/D_2O (62/38)	18.76	30	1.038	0.618	2.07
CM4	H_2O/D_2O (34/66)	19.32	30	1.069	1.197	4
D_2O	D_2O	20	30	1.107	1.9	6.35
			Room-Temperature Ionic Liquids			
[bmim][Cl]	$C_8H_{15}N_2Cl$	174.67	268.57	1.086	2.538	0.951
[Choline][Cl]	$C_5H_{14}NOCl$	139.6	212.68	1.09	0.562	0.264
[bmim]	$C_8H_{15}N_2$	139.27	167		1.580	0.94
[Choline]	$C_5H_{14}NO$	104.2	132		−0.395	−0.298

dx.doi.org/10.1021/jp507631h | J. Phys. Chem. B 2014, 118, 12192−12206

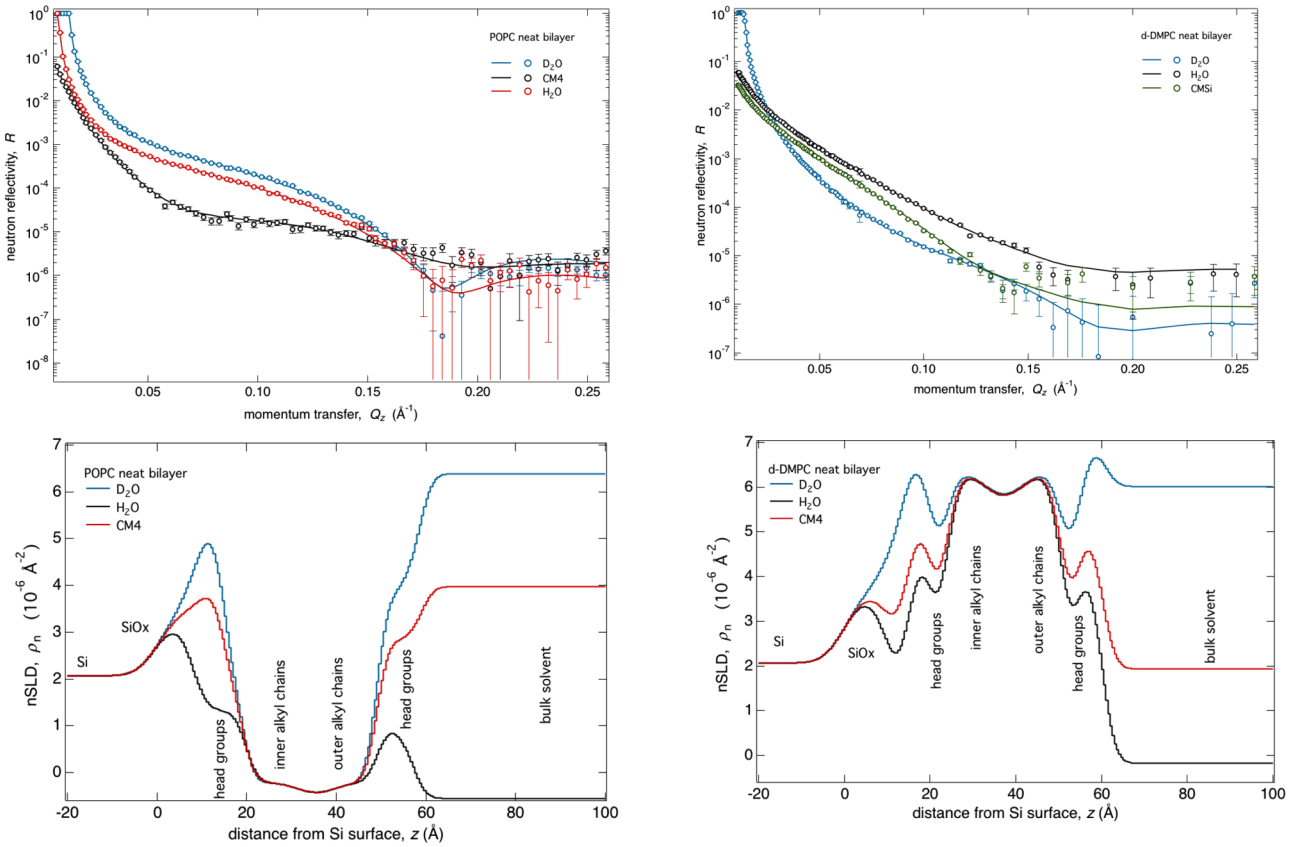

Figure 3. Reflectivity R as a function of the momentum transfer Q_z for two neat bilayers: (a) POPC-n1, measured on MAGIK; (b) d_{67}-DMPC measured on FIGARO. For each bilayer, data were collected at three/four different H/D solvent contrasts (black, blue, red, and dark green empty dots with error bars). The scattering length density profiles reported in (c) (POPC-n1) and (d) (d_{67}-DMPC) were obtained by fitting the reflectivity data. The corresponding best fit to the $R(Q_z)$ curves are displayed as full lines in (a) and (b).

The analysis of the raw data shows that the experimental curves are remarkably well-reproduced by the reflectivity of a planar distribution of scattering length density (SLD) whose profile in the direction perpendicular to the sample is shown in Figure 3c,d. In Figure 1 of the Supporting Information the same profiles for the other two measured systems are shown.

The results of the data analysis, carried out according to the procedure detailed in the previous subsection, are summarized in Table 2, whereas the complete set of the fitting parameters are reported in Table 3 in the main text and in Tables 2 and 3 of the Supporting Information.

As discussed in detail in ref 60, the comparison of even basic structural parameters measured on different samples by a variety of experimental techniques is somewhat uncertain, since different methods do not necessarily measure directly the same quantity, and the sample preparation may affect the result. For instance, our measurements are carried out on single bilayers deposited on a silica substrate, cushioned by a thin water layer. Other measurements, such as X-ray diffraction, nominally for the same system, are carried out on thick stacks of up to 1000 bilayers, separated by a thin hydration layer. Despite these differences, the main structural results provided by our data analysis fall within the range of other measurements, as apparent by comparison of the bilayer width reported in our Table 2 with the data given in ref 61 for POPC and in ref 62 for DMPC.

Most of the quantitative discrepancy with respect to previous measurements on thick lipid stacks might indeed be due to the strong interaction of the inner lipid leaflet with the solid substrate,

Table 2. Thickness, Area Per Lipid, and Bilayer Completeness for Each Neat Bilayer Used in Our Study

	thickness (Å)	area per lipid in outer lipid leaflet (Å^2)	bilayer completeness[a]
POPC n1[b]	45.3 ± 1.1	70.3 ± 3.3	1 ± 0.01
POPC n2[b]	50 ± 0.8	70.2 ± 3.1	1 ± 0.01
DMPC	44.2 ± 0.9	54.8 ± 0.9	0.96 ± 0.02
d_{67}-DMPC	47.6 ± 1	54.1 ± 1.3	0.99 ± 0.02

[a]The error on the bilayer thickness is given by a sum of standard deviations of the corresponding bilayer components. [b]POPC n1 and n2 were used to investigate the effect adding [bmim][Cl] and [Chol][Cl], respectively.

as suggested by sizable difference of structural parameters measured on the inner and on the outer lipid leaflet.

On the other hand, samples of the same phospholipid bilayer (POPC n1 and POPC n2, see Table 2) both made by us to probe different RTILs, display differences in their geometric parameters larger than the error bar estimated by statistical approaches, thus revealing systematic differences in the two bilayers, even though they result from the same experimental protocol. Once again, the interaction with the solid substrate might be responsible for this anomaly, since the difference between the POPC n1 and n2 samples is apparently due to the different thicknesses estimated by NR for the layer of lipid heads in immediate contact with silica.

Similar effects are often seen in phospholipid experiments, and the simultaneous analysis of all the data for a given phospholipid/silica sample with and without RTIL in solution (see Data Analysis Protocol), is meant precisely to overcome this difficulty,

dx.doi.org/10.1021/jp507631h | J. Phys. Chem. B 2014, 118, 12192−12206

Table 3. Markov-Chain Monte Carlo Median Fit Values with 68% Confidence Limit for the POPC+[Chol][Cl] System Measured on MAGIK[a]

	neat bilayer	0.5 mM incubation	rinse
Substrate			
thickness SiOx/Å	8.0 ± 0.8		
nSLD SiOx/10^{-6} Å	3.58 ± 0.16		
substrate roughness/Å	1.5 ± 0.9		
Lipid Bilayer			
thickness submembrane space/Å	0.25 ± 0.4		
thickness inner headgroups/Å	10.1 ± 0.6		
thickness inner lipid leaflet	17.2 ± 0.7	change per leaflet: −0.77 ± 0.33	change per leaflet: −0.31 ± 0.24
thickness outer lipid leaflet	13.2 ± 0.6		
thickness outer headgroups	9.56 fix[b]		
bilayer completeness	1.00 ± 0.01	1.00 ± 0.01	1.00 ± 0.01
area per lipid in outer lipid leaflet/Å^2	70.2 ± 3.1	75.0 ± 4.0	72.3 ± 3.8
RTIL			
volume surface density/(Å^3/Å^2)		3.7 ± 1.7	1.3 + 1.8−0.8[c]
center of mass of RTIL distribution with respect to the outer hydrocarbon/headgroup interface/Å		−3 ± 5	−3 ± 8

[a][Chol][Cl]/water solution at 0.5 M. All measured data sets were analysed simultaneously. The χ^2 value of the fit is 1.79. [b]See ref 52. [c]The error is not symmetric.

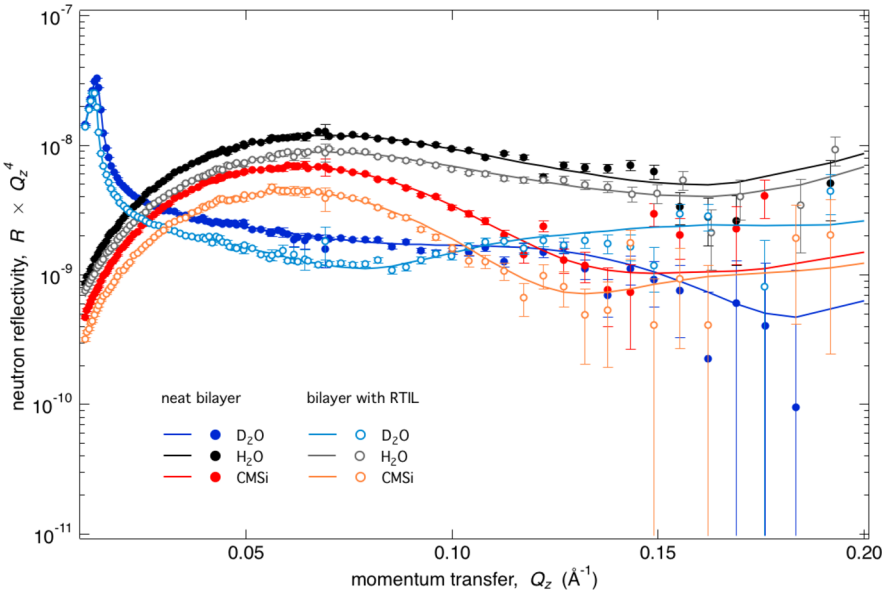

Figure 4. Reflectivity R as a function of the momentum transfer Q_z measured on the neat d_{67}-DMPC bilayer, during the interaction stage with [bmim][Cl] room-temperature ionic liquid. Data for three different H/D solvent contrasts were collected for each of the two (neat, and interaction) stages (black, blue, and red filled and empty dots with error bars). The solid lines are the best fit to the data, shown here as a guide to the eye. The isotopic composition of CMSi is given in Table 1.

compensating systematic errors and enhancing the sensitivity of our measurements with respect to the effects of the RTIL addition.

Moreover, the fair agreement of our structural data with the results of previous measurements lends support to the overall good quality of the bilayers, which is also confirmed by the completeness of the density profile that closely approaches 1 in all cases, as shown in Table 2.

The largest deviation from exact completeness observed in our measurements concerns the neat (i.e., without RTIL) h-DMPC sample whose completeness, although still excellent, is 96%. In neutron-reflectivity measurements, under-completeness is usually attributed to solvent mixing into the bilayer, which in the case of h-DMPC is likely to be responsible for the enhanced penetration and spread of RTIL into DMPC with respect to POPC that is discussed below.

The NR measurements and data analysis carried out on the neat bilayers were repeated upon the addition of the RTIL in the second and major production stage of our study. In practice, the introduction of RTIL is carried out by replacing the pure water solvent in contact with the bilayer by the water solutions of RTILs at 0.1 and 0.5 M concentration. As a term of comparison, we remark that the critical aggregation concentration of [bmim][Cl] in water is 0.8 M.[63] We anticipate that the RTIL concentration in the water solution does not have a major effect on the results, at least over the 0.1−0.5 M range explored by our measurements. The surface density of RTIL molecules absorbed into the lipid phase, in fact, seems to be determined primarily by the direct lipid−cation interaction and possibly by electrostatic double-layer considerations. The chemical potential of cations in solution, on the other hand, has a weak logarithmic dependence

dx.doi.org/10.1021/jp507631h | J. Phys. Chem. B 2014, 118, 12192−12206

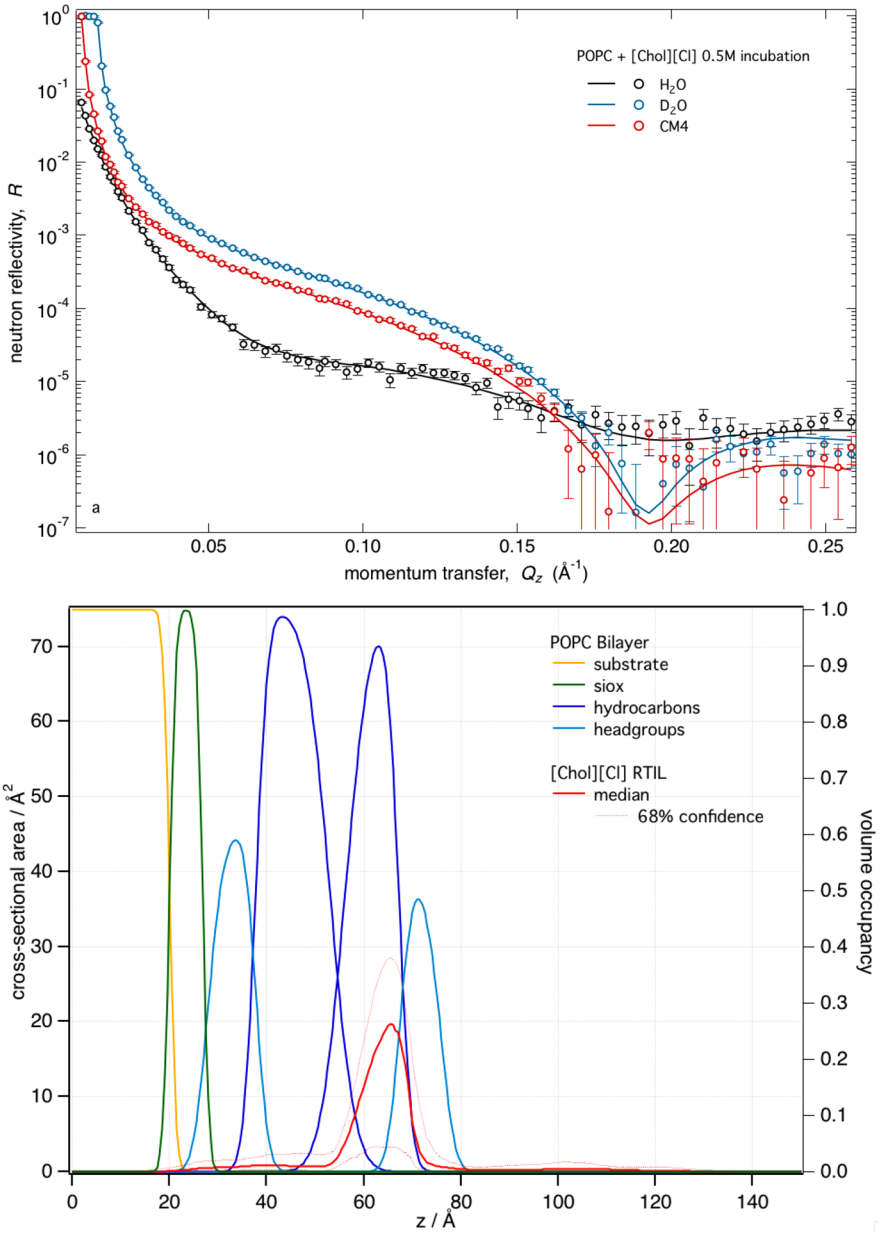

Figure 5. (upper) Reflectivity R as a function of the momentum transfer Q_z measured on POPC after incubation with a 0.5 M [Chol][Cl] water solution. Data for three different H/D solvent contrasts were collected (black, blue, and red empty dots with error bars). The isotopic composition of CM4 is given in Table 1. (lower) Volume occupancy profile as a function of height z from the surface obtained by fitting the reflectivity data. The best fit to the $R(Q_z)$ curves are displayed as full lines in the upper panel. RTIL absorption accounts for 8% of the lipid bilayer volume.

on concentration, limiting its role in the determination of the equilibrium density profile.

Figure 4 compares the reflectivity coefficient $R(Q_z)$ measured on the d_{67}-DMPC bilayer interacting with a water solution of [bmim][Cl] at 0.5 M concentration with the same quantity measured for the neat samples before the RTIL addition. Despite the sizable and systematic separation of these curves, the quantities of interest inferred from the elaboration of these raw data, consisting of the variation of structural parameters for the lipid component, of the mass and volume of adsorbed RTIL and of the density profile of ions along the direction normal to the interface, are affected by important statistical and systematic error bars. As already stated, and repeated here because this is a crucial aspect of our study, the quality of the results is strengthened by the simultaneous fit of all the data measured for a given lipid, considering neat conditions, RTIL additions, and different solvent contrast. Only in this way, exploiting correlations and the cancellation of systematic errors, we can extract statistically significant data for the changes in the lipid layer properties and for the distribution of ions across the interface.

The reflectivity curves as a function of momentum transfer for POPC+[Chol][Cl], POPC+[bmim][Cl], and d_{67}-DMPC +[bmim][Cl], respectively, are shown in the upper panels of Figures 5, 6, and 7. All RTIL solutions are at 0.5 M concentration. Additional figures and data are provided as Supporting Information.

A summary of the structural data obtained in our study is given in Table 4, while a visual representation of the spatial distribution of the various components is provided by the lower panels of Figures 5, 6, and 7. For the complete set of fitting parameters

dx.doi.org/10.1021/jp507631h | J. Phys. Chem. B 2014, 118, 12192−12206

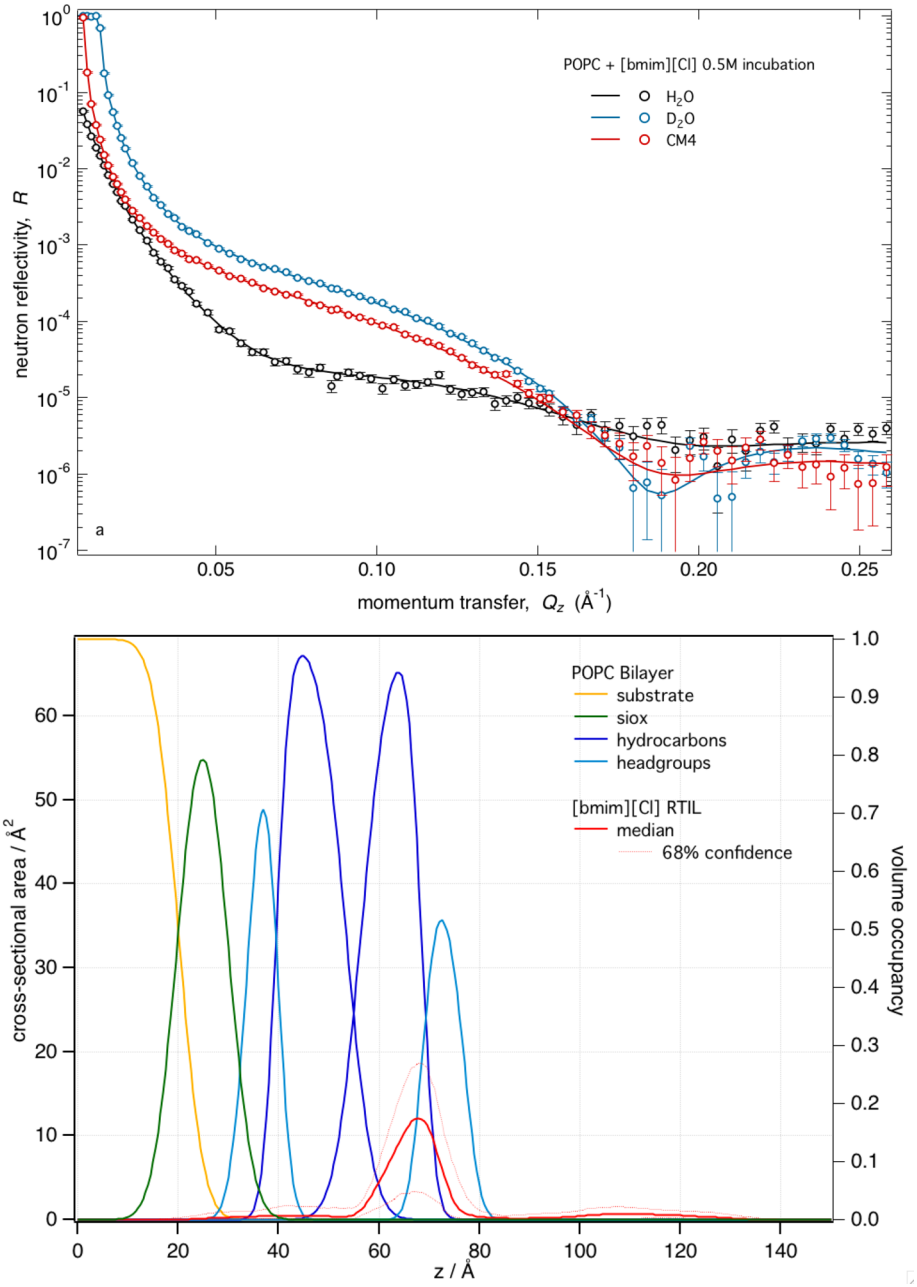

Figure 6. (upper) Reflectivity R as a function of the momentum transfer Q_z measured on POPC after incubation with a 0.5 M [bmim][Cl] water solution. The isotopic composition of CM4 is given in Table 1. (lower) Volume occupancy profile as a function of height z from the surface obtained by fitting the reflectivity data. Lines and symbols as in Figure 5. RTIL absorption accounts for 6.5% of the lipid bilayer volume.

refer to Table 3 in the main text and to Tables 2 and 3 in the Supporting Information.

The first qualitative result, already apparent from inspection of the raw data and, in particular, from the similarity of the reflectivity versus Q_z relation before and after the RTIL addition, is that the bilayers retain their overall integrity upon addition of the RTILs.

Then, the major RTIL effect on the global properties of the lipid component is the apparent shrinking of each bilayer by ∼1 Å, almost irrespective of the lipid and RTIL choice. The shrinkage reported in the Tables represents in fact the variation in the thickness of the tails due to the presence of the RTIL, and it enters the fit as an independent parameter (see Table 3). However, while the thickness of the individual hydrocarbon leaflets is determined separately in the data analysis, only the total variation of the lipid tail thickness can be estimated with acceptable statistical accuracy, while discriminating between the inner and outer leaflet contribution is beyond the reach of our approach. Therefore, a single parameter quantifies this thickness change, and it is applied to both lipid leaflets. The absolute uncertainty on this global thickness change is, not surprisingly, lower than the uncertainty on the absolute thickness of each leaflet.

The completeness, once again approaching 1, confirms the persistence of the basic lipid structure, as well as the good quality of the fit. Even in the h-DMPC case, for which it was down to 0.96 in the neat bilayer case, completeness rises to 1 upon RTIL addition, pointing to a potential ability of RTILs to remove/substitute water or perhaps to enhance the lipid mobility at the interface, thus healing defects of the bilayer. If confirmed, such a

dx.doi.org/10.1021/jp507631h | J. Phys. Chem. B 2014, 118, 12192−12206

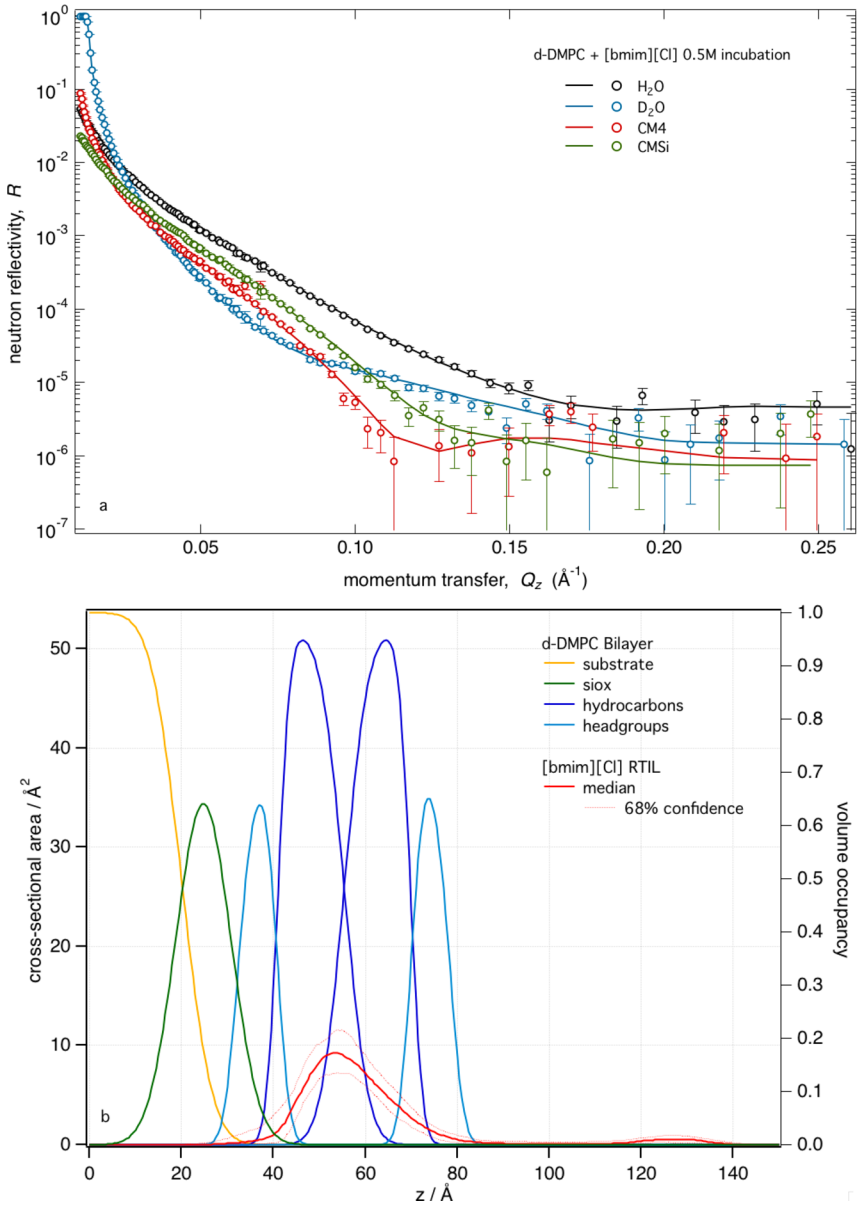

Figure 7. (upper) Reflectivity R as a function of the momentum transfer Q_z measured on d_{67}-DMPC after incubation with a 0.5 M [bmim][Cl] water solution. The isotopic composition of CMSi and CM4 is given in Table 1. (lower) Volume occupancy profile as a function of height z from the surface obtained by fitting the reflectivity data. Lines and symbols as in Figure 5. RTIL absorption accounts for 10% of the lipid bilayer volume.

Table 4. Thickness Variation, Bilayer Completeness, and Ionic Liquid Absorption into the Bilayer after Incubation

	thickness variation[a] (Å)	bilayer completeness[b]	IL per bilayer volume[b] (%)
POPC+[bmim][Cl] (0.1 M)	−0.52 ± 0.28	1 ± 0.01	2.7 ± 2.0
POPC+[bmim][Cl] (0.5 M)	−0.9 ± 0.37	1 ± 0.01	6.4 ± 2.5
POPC+[Chol][Cl] (0.5 M)	−1.5 ± 0.46	1 ± 0.01	8.1 ± 3.9
d-DMPC+[bmim][Cl] (0.5 M)	- 0.42 ± 0.37	0.97 ± 0.05	10.1 ± 1.2
h-DMPC+[bmim][Cl] (0.5 M)	−2.6 ± 0.6	1 ± 0.02	11 ± 3.1

[a]The thickness variation refers to the lipid tails only, because the variation of the headgroup thickness is beyond experimental resolution. Errors are equal to the standard deviation on each parameter value. [b]Errors are equal to the standard deviation on each parameter value.

property could find applications in the preparation and manipulation of lipids and possibly even in pharmacology. On the other hand, the change of completeness in the h-DMPC bilayer before and after the RTIL addition might underlie the difficulty in the determination of the RTIL distribution in space that was discussed in the data analysis subsection.

The apparent shrinkage observed in all our samples occurs at the same time, and it is driven by a non-negligible absorption of ions into the bilayer, as shown by the density profiles obtained through our data analysis (see again the bottom panel in Figures 5, 6, and 7). In other terms, the reduction in the bare lipid volume is even more significant than the nominal shrinking reported in the Tables.

dx.doi.org/10.1021/jp507631h | J. Phys. Chem. B 2014, 118, 12192−12206

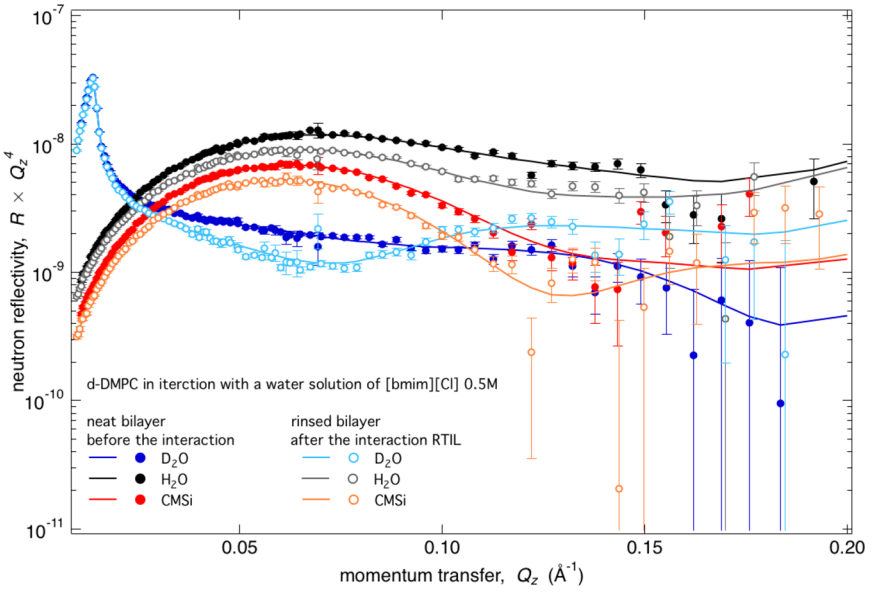

Figure 8. Reflectivity R as a function of the momentum transfer Q_z measured on the neat d_{67}-DMPC bilayer and after the rinsing with pure water. Data for three different H/D solvent contrasts were collected for each of the two (neat, and after rinsing) stages (black, blue, and red filled and empty dots with error bars). The solid lines are the best fits to the data, shown here as a guide to the eye. The isotopic composition of CMSi is given in Table 1.

Integration of the area under the density curves shows that the volume fraction of the lipid bilayer occupied by RTIL ions amounts to 6.5% for POPC+[bmim][Cl], 8% for POPC+[Choline][Cl], 11% for h-DMPC+[bmim][Cl], and 10% for d_{67}-DMPC+[bmim][Cl]. Thus, while the shrinkage of the lipid bilayer by 1 Å seems to be independent of the lipid and RTIL identity, the absorption volume does depend on the lipid, that is, ∼5% for the POPC and 10% for the DMPC. On the other hand our data do not allow us to identify a relationship between the amount of the absorbed RTIL and the RTIL identity. In fact, in the two POPC cases, one with [bmim][Cl] and one with [Chol][Cl], the amount of absorbed RTIL is almost the same taking into account the experimental and statistical error. The combination of shrinking and absorption, of course, implies an increase of the bilayer density that increases with the volume fraction occupied by the RTIL. Thus, this same volume fraction might provide a measure for the affinity of RTIL and lipids. Once calibrated, such a scale could find applications in pharmacology and in sensing.

The molecular distribution curves (lower panels of Figures 5, 6, and 7) give us information not only on the amount of the RTIL in the bilayer but also on its location within the bilayer. A first qualitative observation is that, despite some variations, the peak of the RTIL density tends to be located within the neutral portion of the leaflet exposed to the RTIL solution, and the overlap with the lipid head distribution is limited. This observation suggests that van der Waals (dispersion) rather than Coulomb interactions represent the driving force for the ion absorption into the lipid bilayer. Molecular dynamics simulations[41,42] for [bmim][Cl] interacting with POPC bilayers, for instance, show that short-range repulsion and dispersion forces cause the alignment of the absorbed $[bmim]^+$ ions along the direction perpendicular to the bilayer plane and define a preferred location for their absorption within the lipid phase. Given the high charge and fairly low dispersion potential of the $[Cl]^-$ ion, it is tempting to assume that the RTIL density identified by the NR data analysis accounts mainly for the distribution of cations.

To provide a visual impression of the global uncertainty in the determination of the RTIL distribution, we computed all the profiles of equal RTIL content, compatible with the optimal distribution to within the 68% confidence level. The upper and lower envelopes of all these profiles are shown together with each RTIL distribution in Figures 5, 6, and 7. These curves, however, must be interpreted with some care. In particular, one should not conclude from the near vanishing of the lower envelope over its entire range that a null RTIL distribution is compatible with our NR data, since all the density profiles used to define the envelopes correspond to the same total RTIL absorption, that is, 5% in volume for POPC and 10% in volume for DMPC. In fact, the separation of the lower and upper envelopes measures primarily the uncertainty in the RTIL location within the lipid bilayer and does not represent an error bar on the amount of adsorbed RTIL, which is instead given in Table 4.

The h-DMPC sample, whose deviation from full completeness was already noted for the neat bilayers, is somewhat anomalous also for what concerns the location of the RTIL upon absorption. While in the POPC case both $[bmim]^+$ and $[Chol]^+$ are confined to the outer lipid leaflet, a non-negligible penetration into the inner leaflet is observed for h-DMPC (see the leftmost peak in the RTIL distribution of Figure 3 in the Supporting Information). Taking into account the confidence curves, this amount could represent one-fourth of the adsorbed RTIL, or 2−3% of the h-DMPC volume. The two peculiar behaviors displayed by this bilayer are likely to be related, since it might be precisely the lower completeness of h-DMPC and partial water penetration into the lipid that opens the way to RTIL diffusion. Another possible interpretation is that both under-completeness of the neat bilayer and the higher RTIL penetration are both due to the lipid interaction with the substrate, which in the absence of RTIL might prevent the lateral diffusion of lipids and limit their packing in the inner leaflet. We are unable, right now, to distinguish between these two different possibilities. More importantly, and also more in general, on the basis of our data alone we are unable to conclude

dx.doi.org/10.1021/jp507631h | J. Phys. Chem. B 2014, 118, 12192−12206

Table 5. Thickness Variation, Bilayer Completeness, and Ionic Liquid Absorption into the Bilayer for All the Samples after Rinsing with Pure Water

	thickness variation[a] (A)	bilayer completeness[a]	IL per bilayer volume[a] (%)
POPC+[bmim][Cl] (0.1 M)	−1.54 ± 0.32	1 ± 0.01	5.8 ± 2.4
POPC+[bmim][Cl] (0.5 M)	−1 ± 0.35	1 ± 0.01	2.5 ± 1.8
POPC+[Chol][Cl] (0.5 M)	−0.62 ± 0.34	1 ± 0.01	2.3 ± 1.4
d-DMPC+[bmim][Cl] (0.5 M)	1 ± 0.23	0.99 ± 0.05	8 ± 1.1
h-DMPC+[bmim][Cl] (0.5 M)	−2.8 ± 0.7	0.99 ± 0.02	17.1 ± 5.2

[a]Errors are equal to the standard deviation on each parameter value.

whether the RTIL distribution measured in our NR experiments is an equilibrium property or is primarily determined by kinetics.

In a third and last stage of our measurements, the RTIL water solution was replaced again by pure water, rinsing each experimental cell with ∼10 mL of pure water. Qualitative inspection of the NR curves at different H/D contrasts shows that rinsing and equilibrating the system in pure water does not restore the neat bilayer geometry seen before the RTIL introduction, implying that the modifications induced by the RTIL absorption are to some extent irreversible (Figure 8). Quantitative fit of the raw NR data by continuous density distributions show that, in fact, the RTIL absorption and location into the bilayer are only slightly affected by equilibration in the new solvent (pure water) over macroscopic times. Integrating again the ion density distributions, we estimate that, after rinsing with pure water, the bilayer volume occupied by the RTIL amounts to 2.5% for both POPC+[bmim][Cl] and POPC+[choline][Cl]; 17.1% for h-DMPC+[bmim][Cl]; and 8% for d_{67}-DMPC+[bmim][Cl]. Despite some quantitative variations, the similarity with the previous results confirm the partial irreversibility of the RTIL absorption into the phospholipid bilayer.

The results for the fit of the NR data on samples after rinsing are summarized in Table 5, whereas the complete set of fit parameter are shown in Table 3 for the POPC+[Chol][Cl] and in the Supporting Information for all the other systems, together with the NR curves and the volume occupancy distribution curves.

Two unexpected features are apparent in the results obtained after rinsing with pure water: (a) for the h-DMPC, the amount of RTIL is higher after rinsing than before rinsing, and (b) for the d_{67}-DMPC the bilayer thickness increases by ∼1 Å upon rinsing. Both results are affected by large error bars and are likely to result from fluctuations. For this reason we do not attempt to give an explanation for them.

CONCLUSION

The interaction between two prototypical RTIL water solutions, namely,[bmim][Cl] and [Chol][Cl], with two bilayers made of POPC and DMPC phospholipids deposited on a silica substrate, has been investigated by NR measurements in the specular reflection mode. Contrast variation obtained by isotopic substitution in the solvent (water) and in the lipids has been used to separate the contribution of the solid substrate, of the lipid heads and tails, of the RTILs, and of the solvent. The composition-space approach[52] has been used to convert the raw data represented by the reflectivity coefficient R as a function of momentum transfer Q_z into the density distribution of the various chemical species along the normal to the solid/fluid interface, measured at subnanometer resolution. The error bars on the structural parameters obtained in this way have been estimated by a Markov chain Monte Carlo procedure.

The first and foremost result of our study is that specular NR coupled to state-of-the-art data analysis allows us to estimate the amount of RTIL absorbed into the lipid phase and thus to confirm the high affinity of phospholipids and RTIL cations, already suggested by experiments[37−39] and by computer simulations.[41,42] Our results allow us to determine also the RTIL preferred location within the bilayer. Admittedly, the determination of the RTIL distribution in the lipid phase is at the limit of the accuracy offered by our approach, but statistical inference and the regularity of the trends among the measurements on the different samples give us confidence on the significance of our results. The overall agreement of our data for the neat bilayers with benchmark results in the literature[61,62] further enhances our confidence.

Because of numerical reasons, we could not independently determine the distribution of cations and anions. However, since the $[Cl]^-$ anion is generally insoluble in lipids, we assume that the RTIL distribution in the lipid bilayer represents the density of cations only. Our analysis of NR data implicitly depends on this assumption, since in the fits we always use the cation SLD instead of the molecular (cation plus anion) one.

A more detailed summary of our results is as follows: (a) The basic structure of the phospholipid membranes does not change significantly upon addition of the RTIL in solution at 0.1−0.5 M concentration, the major difference in the structural parameters being an ∼1 Å reduction in the bilayer thickness of all samples; the bilayer completeness before and after the lipid bilayer incubation in the RTIL/water solution is almost 100% for all the systems, confirming the in-plane regularity of the bilayer and the good quality of our fit. (b) The cation of the RTILs penetrates into the nonpolar region of the bilayer, and in the few cases that we analyzed, its final distribution does not seem to be dependent either on the cation or lipid choice. (c) The amount of RTIL absorbed into the bilayer, instead, depends on the lipid, ranging from 5% of the total bilayer volume for POPC to 10% for DMPC. (d) The penetration of the RTILs into the bilayer is at least partially irreversible, and a measurable amount of RTIL (2.5% for POPC and 8% for DMPC) remains absorbed into the lipid phase after rinsing in pure water the samples equilibrated in the RTIL/water solution. (e) In the 0.1−0.5 M range, the RTIL concentration in solution does not affect much the local picture of the RTIL/lipid association. Short-range cation−lipid interactions, and perhaps electrostatic forces at the lipid−water interface, affect the RTIL distribution far more than the weak logarithmic dependence of the cation chemical potential on the RTIL concentration in solution.

The thinning of the bilayer upon addition of a third species that is at least partly sorbed into/onto the lipid phase is somewhat counterintuitive but not without previous examples. References 64 and 65 for instance, report the thinning of phospholipid membranes following the adsorption of peptides at the lipid/water interface. Reference 64, in particular, proposes a

mechanism for thinning based on the expansion of the area covered, on average, by each lipid headgroup, causing the shrinking of the width to conserve the lipid volume.

Our data on the distribution of cations across the bilayer, showing a significant penetration into the bilayer, point to a different mechanism, or, more likely, to the combination of two mechanisms. Molecular simulation data[40−43] for [bmim][Cl], for instance, show that RTIL cations enter the bilayer with an orientation that optimizes the close contact of their most ionic portion (imidazolium) with the lipid polar heads, while their least ionic portion, represented by the butyl chain, is solvated by the hydrophobic lipid tails. According to this picture, the imidazolium moiety of $[bmim]^+$ might cause the bilayer thinning by the same mechanism as that of ref 65, while the butyl tail of these same molecules might partly compensate this dominant effect[41,42] by mixing with the neutral lipid tails. Unfortunately, no modeling and simulation result is available for [Chol][Cl].

Because of the high contrast between the RTIL and the lipid scattering length density, the most accurate determination of the RTIL location into the bilayer has been obtained for the d_{67}-DMPC system. The least significant results turned out to be those for h-DMPC, possibly because of a defective bilayer formation in the first stages of the sample preparation. For this reason, the RTIL distribution in h-DMPC shown in Figure 3 of the Supporting Information might be affected by systematic errors that we are unable to fully quantify. The same warning concerns also the broad peak located well above the lipid range, at 120 < z/Å < 150, as shown in Figure 3 of the Supporting Information.

Our analysis, focusing on the changes of structural parameters due to the $[bmim]^+$ and $[Chol]^+$ sorption in/on the bilayer, could achieve angstrom-scale resolution from measurements whose absolute accuracy is in, approximately, the nanometer range. A significantly better determination of cation and anion distributions, or the estimation of further geometrical parameters, would require angstrom-scale resolution for the absolute structural determination. At present, this is prevented by limitations in the range of Q_z momenta accessible by the experiment and also by the homogeneity and reproducibility of the samples. On the short time scale, progress could more likely be expected from the combination of different approaches, such as other neutron-scattering techniques, photoluminescence and spectroscopy, as well as computer modeling.

The overall stability of the bilayers upon RTIL addition might seem at odds with the results of refs 37 and 38, reporting significant damage on phospholipid bilayers in contact with water solutions of $[C_n mim][Cl]$, with n = 4, 6, and 8. However, neglecting the slight difference in the phospholipids used in the present and past investigations, a careful comparison of results reveals many more points of agreement than of disagreement. For instance, previous studies reported extensive damage of the bilayer only for $[C_n mim]^+$ cations with n = 6 and n = 8,[37−39] whose interaction with the lipid tails through dispersion interactions is strong. RTILs based on $[bmim]^+$ (n = 4) instead, displayed only limited absorption[37] and caused leakage only from localized holes on the bilayers.[38]

This is certainly compatible with our observations, displaying an absorption of RTIL into the lipid limited to ∼10%. Moreover, the absorption of all RTILs, including [bmim][Cl], has been shown to be irreversible,[39] again in agreement with our results. Residual differences between our data and the results of AFM imaging[38] could also be due to the measurement method, since AFM locally interacts strongly with lipid and RTIL molecules, while NR really represents only a weak perturbation for the bilayer.

We are unable, at present, to unambiguously state whether our results for the RTIL distribution within the lipid phase reflect a true equilibrium state or result from kinetic constraints. NR measurements, however, last several hours, and the fair resolution of the RTIL density profiles shows that a near-equilibrium state is reached fairly soon and persists over macroscopic times.

Our interest in the interaction of RTILs and phospholipid bilayers obviously is due to the role of the latter as primary components of biomembranes. Thus, the experimental analysis of the incorporation of RTILs into phospholipid bilayers provides a way to understand and perhaps predict biological effects of RTILs, with implications in toxicology, environmental sciences, and even pharmacology, given the observed antimicrobial effects of selected RTILs. NR measurements, in particular, could provide also the quantitative basis for novel biotechnological applications in which, for example, molecules and nanoparticles could be inserted into or exchanged through biomembranes using RTILs as surfactants and driving agents.

■ ASSOCIATED CONTENT

Supporting Information

Tables with lists of all samples considered in the measurements; optimal parameters from the fit of NR data; neutron reflectivity curves, and corresponding volume occupancy profiles as a function of height z from the solid silica surface. This material is available free of charge via the Internet at http://pubs.acs.org.

■ AUTHOR INFORMATION

Corresponding Author

*E-mail: antonio.benedetto@ucd.ie. Phone: +353 (0)1 716 1794.

Notes

The authors declare no competing financial interest.

Certain commercial materials, equipment, and instruments are identified in this manuscript in order to specify the experimental procedure as completely as possible. In no case does such an identification imply a recommendation or endorsement by the National Institute of Standards and Technology, nor does it imply that the materials, equipment, or instruments identified are necessarily the best available for the purpose.

■ ACKNOWLEDGMENTS

A.B. acknowledges the support from the European Union under a Marie Curie Intra-European Fellowship for Career Development (IEF) within the seventh European Community Framework Programme (Grant HYDRA No. 301463). P.B. acknowledges support from the Istituto Italiano di Tecnologia (IIT) under the SEED project SIMBEDD Grant No. 259. The authors wish to acknowledge both the Institute of National Standard and Technology, Gaithersburg, USA, and the Institut Laue-Langevin, Grenoble, France, for the beam time on MAGIK and FIGARO reflectrometers, respectively, and the PSCM @ ILL.

■ REFERENCES

(1) Welton, T. Room-Temperature Ionic Liquids. Solvents for Synthesis and Catalysis. *Chem. Rev.* **1999**, *99*, 2071−2084.

(2) *Ionic Liquids: From Knowledge to Applications;* Plechkova, N. V., Rogers, R. D., Seddon, K. R., Eds.; ACS Symposium Series 1030; American Chemical Society: Washington, DC, USA, 2009.

(3) Brennecke, J. F.; Maginn, E. J. Ionic Liquids: Innovative Fluids for Chemical Processing. *AIChE J.* **2001**, *47*, 2384−2389.

(4) Hallett, J. P.; Welton, T. Room-Temperature Ionic Liquids: Solvents for Synthesis and Catalysis. 2. *Chem. Rev.* **2011**, *111*, 3508−3576.
(5) Dupont, J.; de Souza, R. F.; Suarez, P. A. Z. Ionic Liquid (Molten Salt) Phase Organometallic Catalysis. *Chem. Rev.* **2002**, *102*, 3667−3692.
(6) Ye, C.; Liu, W.; Chen, T.; Yu, L. Room-Temperature Ionic Liquids: a Novel Versatile Lubricant. *Chem. Commun.* **2001**, 2244−2245.
(7) Minami, I. Ionic Liquids in Tribology. *Molecules* **2009**, *14*, 2286−2305.
(8) Howlett, P. C.; MacFarlane, D. R.; Hollenkamp, A. F. High Lithium Metal Cycling Efficiency in a Room Temperature Ionic Liquid. *Electrochem. Solid-State Lett.* **2004**, *7*, A97−A101.
(9) Torimoto, T.; Tsuda, T.; Okazaki, K.; Kuwabata, S. New Frontiers in Materials Science Opened by Ionic Liquids. *Adv. Mater.* **2010**, *22*, 1196−1221.
(10) Bonhôte, P.; Dias, A. P.; Papageorgiou, N.; Kalyanasundaram, K.; Grätzel, M. Hydrophobic, Highly Conductive Ambient-Temperature Molten Salts. *Inorg. Chem.* **1996**, *35*, 1168−1178.
(11) Wang, P.; Zakeeruddin, S. M.; Exnar, I.; Grätzel, M. High Efficiency Dye-Sensitized Nanocrystalline Solar Cells Based on Gel Electrolyte. *Chem. Commun.* **2002**, 2972−2973.
(12) Gurkan, B.; Goodrich, B. F.; Mindrup, E. M.; Ficke, L. E.; Massel, M.; Seo, S.; Senftle, T. P.; Wu, H.; Glaser, M. F.; Shah, J. K.; et al. Molecular Design of High Capacity, Low Viscosity, Chemically Tunable Ionic Liquids for CO_2 Capture. *J. Phys. Chem. Lett.* **2010**, *1*, 3494−3499.
(13) Plechkova, N. V.; Seddon, K. R. Applications of Ionic Liquids in the Chemical Industry. *Chem. Soc. Rev.* **2008**, *37*, 123−150.
(14) Holbrey, J. D.; Seddon, K. R. Ionic Liquids. *Clean Prod. Processes* **1999**, *1*, 223−236.
(15) Earle, M. J.; McCormac, P. B.; Seddon, K. R. Diels−Alder Reactions in Ionic Liquids. A Safe Recyclable Alternative to Lithium Perchlorate−Diethyl Ether Mixtures. *Green Chem.* **1999**, *1*, 23−25.
(16) Hough, W. L.; Smiglak, M.; Rodriguez, H.; Swatloski, R. P.; Spear, S. K.; Daly, D. T.; Pernak, J.; Grisel, J. E.; Carliss, R. D.; Soutullo, M. D.; et al. The Third Evolution of Ionic Liquids: Active Pharmaceutical Ingredients. *New J. Chem.* **2007**, *31*, 1429−1436.
(17) Petkovic, M.; Seddon, K. R.; Rebelo, L. P. N.; Pereira, C. S. Ionic Liquids: a Pathway to Environmental Acceptability. *Chem. Soc. Rev.* **2011**, *40*, 1383−1403.
(18) Stolte, S.; Arning, J.; Bottin-Weber, U.; Matzke, M.; Stock, F.; Thiele, K.; Uerdingen, M.; Welz-Bierman, U.; Jastorff, B.; Ranke, J. Anion Effects on the Cytotoxicity of Ionic Liquids. *Green Chem.* **2006**, *8*, 621−629.
(19) Viboud, S.; Papaiconomou, N.; Cortesi, A.; Chatel, G.; Draye, M.; Fontvieille, D. Correlating the Structure and Composition of Ionic Liquids with their Toxicity on Vibrio Fischeri: A Systematic Study. *J. Hazard. Mater.* **2012**, *215−216*, 40−48.
(20) Pretti, C.; Chiappe, C.; Pieraccini, D.; Gregori, M.; Abramo, F.; Monnia, G.; Intorre, L. Acute Toxicity of Ionic Liquids to the Zebrafish (Danio Rerio). *Green Chem.* **2006**, *8*, 238−240.
(21) Bernot, R. J.; Brueseke, M. A.; Evans-White, M. A.; Lamberti, G. A. Acute and Chronic Toxicity of Imidazolium-Based Ionic Liquids on Daphnia Magna. *Environ. Toxicol. Chem.* **2005**, *24*, 87−92.
(22) O'Toole, G. A.; Wathier, M.; Zegans, M. E.; Shanks, R. M. Q.; Kowalski, R.; Grinstaff, M. W. Diphosphonium Ionic Liquids as Broad Spectrum Antimicrobial Agents. *Cornea* **2012**, *31*, 810−816.
(23) Pernak, J.; Goc, I.; Mirska, I. Anti-Microbial Activities of Protic Ionic Liquids with Lactate Anion. *Green Chem.* **2004**, *6*, 323−329.
(24) Pernak, J.; Sobaszkiewicz, K.; Mirska, I. Anti-Microbial Activities of Ionic Liquids. *Green Chem.* **2003**, *5*, 52−56.
(25) Demberelnyamba, D.; Kim, K. S.; Choi, S.; Park, S.-Y.; Lee, H.; Kim, C.-J.; Yoo, I.-D. Synthesis and Antimicrobial Properties of Imidazolium and Pyrrolidinonium Salts. *Bioorg. Med. Chem.* **2004**, *12*, 853−857.
(26) Docherty, K. M.; Kulpa, C. F. Toxicity and Antimicrobial Activity of Imidazolium and Pyridinium Ionic Liquids. *Green Chem.* **2005**, *7*, 185−189.
(27) Salminen, J.; Papaiconomou, N.; Kumar, R. A.; Lee, J.-M.; Kerr, J.; Newman, J.; Prausnitz, J. M. Physicochemical Properties and Toxicities of Hydrophobic Piperidinium and Pyrrolidinium Ionic Liquids. *Fluid Phase Equilib.* **2007**, 421−426.
(28) Laszlo, J. A.; Compton, D. L. Comparison of Peroxidase Activities of Hemin, Cytochrome C and Microperoxidase-11 in Molecular Solvents and Imidazolium-Based Ionic Liquids. *J. Mol. Catal. B: Enzym.* **2002**, *18*, 109−120.
(29) DiCarlo, C. M.; Compton, D. L.; Evans, K. O.; Laszlo, J. A. Bioelectrocatalysis in Ionic Liquids. Examining Specific Cation and Anion Effects on Electrode-Immobilized Cytochrome C. *Bioelectrochemistry* **2006**, *68*, 134−143.
(30) Laszlo, J. A.; Compton, D. L. Characterization of the [Ru(CN)5(pyS)]4− Ion Complex Adsorbed on Gold, Silver and Copper Substrates by Surface-Enhanced Raman Spectroscopy. *J. Electroanal. Chem.* **2002**, *520*, 71−78.
(31) Byrne, N.; Angell, C. A. Formation and Dissolution of Hen Egg White Amyloid in Protic Ionic Liquids. *Chem. Commun.* **2009**, 1046−1048.
(32) Kalhor, H. R.; Kamizi, M.; Akbari, J.; Heydari, A. Inhibition of Amyloid Formation by Ionic Liquids: Ionic Liquids Affecting Intermediate Oligomers. *Biomacromolecules* **2009**, *10*, 2468−2475.
(33) Gras, S. L.; Tickler, A. K.; Squires, A. M.; Devlin, G. L.; Horton, M. A.; Dobson, C. M.; MacPhee, C. E. Functionalised Amyloid Fibrils for Roles in Cell Adhesion. *Biomaterials* **2008**, *29*, 1553−1562.
(34) Portella, G.; Germann, M. W.; Hud, N. V.; Orozco, M. MD and NMR Analyses of Choline and TMA Binding to Duplex DNA: On the Origins of Aberrant Sequence-Dependent Stability by Alkyl Cations in Aqueous and Water-Free Solvents. *J. Am. Chem. Soc.* **2014**, *136*, 3075−3086.
(35) Vijayaraghavan, R.; Izgorodin, A.; Ganesh, V.; Surianarayanan, M.; MacFarlane, D. R. Long-Term Structural and Chemical Stability of DNA in Hydrated Ionic Liquids. *Angew. Chem., Int. Ed.* **2010**, *49*, 1631−1633.
(36) Jeong, S.; Ha, S. O.; Han, S.-H.; Lim, M.-C.; Kim, S. M.; Kim, Y.-R.; Koo, Y.-M.; So, J.-S.; Jeon, T.-J. Elucidation of Molecular Interactions Between Membranes and Using Model Cell Membranes. *Soft Matter* **2012**, *8*, 5501−5506.
(37) Evans, K. O. Supported Phospholipid Bilayer Interaction with Components Found in Typical Room Temperature Ionic Liquids a QCM-D and AFM Study. *Int. J. Mol. Sci.* **2008**, *9*, 498−511.
(38) Evans, K. O. Room-Temperature Ionic Liquid Cations Act as Short-Chain Surfactants and Disintegrate a Phospholipid Bilayer. *Colloids Surf., A* **2006**, *274*, 11−17.
(39) Evans, K. O. Supported Phospholipid Membrane Interactions with 1-Butyl-3-methyl-imidazolium Chloride. *J. Phys. Chem. B* **2008**, *112*, 8558−8562.
(40) Cromie, S. R. T.; Del Popolo, M. G.; Ballone, P. Interaction of Room Temperature Ionic Liquid Solutions with a Cholesterol Bilayer. *J. Phys. Chem. B* **2009**, *113*, 11642−11648.
(41) Bingham, R. J.; Ballone, P. Computational Study of Room-Temperature Ionic Liquids Interacting with a POPC Phospholipid Bilayers. *J. Phys. Chem. B* **2012**, *116*, 11205−11216.
(42) Yoo, B.; Shah, J. K.; Zhu, Y.; Maginn, E. J. Amphiphilic Interactions of Ionic Liquids with Lipid Biomembranes: a Molecular Simulation Study. *Soft Matter* DOI: 10.1039/C4SM01528B in press.
(43) Lim, G. S.; Zidar, J.; Cheong, D. W.; Jaenicke, S.; Klähn, M. Impact of Ionic Liquids in Aqueous Solution on Bacterial Plasma Membranes Studied with Molecular Dynamics Simulations. *J. Phys. Chem. B* **2014**, *118*, 10444−10459.
(44) Johnson, S. J.; Bayerl, T. M.; McDermott, D. C.; Adam, G. W.; Rennie, A. R.; Thomas, R. K.; Sackmann, E. Structure of an Adsorbed Dimyristoylphosphatidylcholine Bilayer Measured with Specular Reflection of Neutrons. *Biophys. J.* **1991**, *59*, 289−294.
(45) Fragneto, G. Neutrons and Model Membranes. *Eur. Phys. J. Special Topics* **2012**, *213*, 327−342.
(46) POPC: 1-palmitoyl-2-oleoyl-*sn*-glycero-3-phosphocholine; DMPC: 1,2-dimyristoyl-*sn*-glycero-3-phosphatidylcholine.

(47) Dura, J. A.; Pierce, D. J.; Majkrzak, C. F.; Maliszewsky, N. C.; McGillivray, D. J.; Lösche, M.; O'Donovan, K. V.; Mihailescu, M.; Perez-Salas, U.; Worchester, D. L.; et al. AND/R: Advanced Neutron Diffractometer/Reflectometer for Investigation of Thin Films and Multilayers for the Life Sciences. *Rev. Sci. Instrum.* **2006**, *77*, 74301−11.
(48) Campbell, R. A.; Wacklin, H. P.; Sutton, I.; Cubitt, R.; Fragneto, G. FIGARO: The New Horizontal Neutron Reflectometer at the ILL. *Eur. Phys. J. Plus* **2011**, *126*, 107.
(49) Penfold, J.; Thomas, R. K. The Application of the Specular Reflection of Neutrons to the Study of Surfaces and Interfaces. *J. Phys.: Condens. Matter* **1990**, *2*, 1369−1412.
(50) Blasie, J. K.; Zheng, S.; Strzalka, J. Solution to the Phase Problem for Specular X-Ray or Neutron Reflectivity fron Thin Films on Liquid Surfaces. *Phys. Rev. B* **2003**, *67*, 224201.
(51) Born, M.; Wolf, E. *Principles of Optics,* 6th ed.; Pergamon: Oxford, U.K., 1989.
(52) Shekhar, P.; Nanda, H.; Lösche, M.; Heinrich, F. Continuous Distribution Model for the Investigation of Complex Molecular Architectures Near Interfaces with Scattering Techniques. *J. Appl. Phys.* **2011**, *110*, 102216.
(53) Shenoy, S.; Shekhar, P.; Heinrich, F.; Daou, M.-C.; Gericke, A.; Ross, A. H.; Lösche, M. Membrane Association of the PTEN Tumor Suppressor: Molecular Details of the Protein-Membrane Complex from SPR Binding Studies and Neutron Reflection. *PLoS One* **2012**, *7*, e32591.
(54) Heinrich, F. J.; Lösche, M. Zooming in on disordered systems: Neutron reflection studies of proteins associated with fluid membranes. *Biochim. Biophys. Acta, Biomembr.* **2014**, *1838*, 2341−2349.
(55) Kienzle, P. A.; Doucet, M.; McGillivray, D. J.; O'Donovan, K. V.; Berk, N. F.; Majkrzak, C. F. 2000−2006. http://www.ncnr.nist.gov/reflpak/garefl.html.
(56) Kirby, B. J.; Kienzle, P. A.; Maranville, B. B.; Berk, N. F.; Krycka, J.; Heinrich, F.; Majkrzak, C. F. Phase-Sensitive Specular Neutron Reflectometry for Imaging the Nanometer Scale Composition Depth Profile of Thin-Film Materials. *Curr. Opin. Colloid Interface Sci.* **2012**, *17*, 44−53.
(57) Petrache, H. I.; Feller, S. E.; Nagle, J. F. Determination of Component Volumes of Lipid Bilayers from Simulations. *Biophys. J.* **1997**, *72*, 2237−2242.
(58) Armen, R. S.; Uitto, O. D.; Feller, S. E. Phospholipid Component Volumes: Determination and Application to Bilayer Structure Calculations. *Biophys. J.* **1998**, *75*, 734−744.
(59) Koenig, B. W.; Gawrisch, K. Specific Volumes of Unsaturated Phosphatidyl -Cholines in the Liquid Crystalline Lamellar Phase. *Biochem. Biophys. Acta* **2005**, *1715*, 65−70.
(60) Nagle, J. F.; Tristam-Nagle, S. Lipid Bilayer Structure. *Curr. Opin. Struct. Biol.* **2000**, *10*, 474−480.
(61) Kučerka, N.; Tristram-Nagle, S.; Nagle, J. F. Structure of Fully Hydrated Fluid Phase Lipid Bilayers with Monounsaturated Chains. *J. Membr. Biol.* **2005**, *208*, 193−202.
(62) Nagle, J. F.; Tristram-Nagle, S. Structure of Lipid Bilayers. *Biochim. Biophys. Acta* **2000**, *1469*, 159−195.
(63) Bowers, J.; Butts, C. P.; Martin, P. J.; Vergara-Gutierrez, M. C.; Heenan, R. K. Aggregation Behavior of Aqueous Solutions of Ionic Liquids. *Langmuir* **2004**, *20*, 2191−2198.
(64) Ludtke, S.; He, K.; Huang, H. Membrane Thinning Caused by Magainin 2. *Biochemistry* **1995**, *34*, 16764−16769.
(65) Hung, W.-C.; Chen, F.-Y.; Lee, C.-C.; Sun, Y.; Lee, M.-T.; Huang, H. W. Membrane-Thinning Effect of Curcumin. *Biophys. J.* **2008**, *94*, 4331−4338.